THE UNIVERSITY OF ALABAMA® | University Libraries

Multiwavelength Follow-up Observations of the Tidal Disruption Event Candidate 2XMMi J184725.1-631724

Jimmy A. Irwin – University of Alabama

et al.

Deposited 12/05/2018

Multiwavelength follow-up observations of the tidal disruption event candidate 2XMMi J184725.1−631724

Dacheng Lin,[1]* Jay Strader,[2] Eleazar R. Carrasco,[3] Olivier Godet,[4,5] Dirk Grupe,[6] Natalie A. Webb,[4,5] Didier Barret[4,5] and Jimmy A. Irwin[7,8]

[1]*Space Science Center, University of New Hampshire, Durham, NH 03824, USA*
[2]*Center for Data Intensive and Time Domain Astronomy, Department of Physics and Astronomy, Michigan State University, 567 Wilson Road, East Lansing, MI 48824, USA*
[3]*Gemini Observatory/AURA, Southern Operations Center, Casilla 603, La Serena, Chile*
[4]*CNRS, IRAP, 9 avenue du Colonel Roche, BP 44346, F-31028 Toulouse Cedex 4, France*
[5]*Université de Toulouse, UPS-OMP, IRAP, Toulouse, France*
[6]*Space Science Center, Morehead State University, 235 Martindale Drive, Morehead, KY 40351, USA*
[7]*Department of Physics and Astronomy, University of Alabama, Box 870324, Tuscaloosa, AL 35487, USA*
[8]*Department of Physics and Astronomy, Seoul National University, Seoul 08826, Korea*

ABSTRACT

The ultrasoft X-ray flare 2XMMi J184725.1−631724 was serendipitously detected in two *XMM–Newton* observations in 2006 and 2007, with a peak luminosity of 6×10^{43} erg s^{-1}. It was suggested to be a tidal disruption event (TDE) because its position is consistent with the centre of an inactive galaxy. It is the only known X-ray TDE candidate whose X-ray spectra showed evidence of a weak steep power-law component besides a dominant supersoft thermal disc. We have carried out multiwavelength follow-up observations of the event. Multiple X-ray monitorings show that the X-ray luminosity has decayed significantly after 2011. Especially, in our deep *Chandra* observation in 2013, we detected a very faint counterpart that supports the nuclear origin of 2XMMi J184725.1−631724 but had an X-ray flux a factor of ∼1000 lower than in the peak of the event. Compared with follow-up ultraviolet (UV) observations, we found that there might be some enhanced UV emission associated with the TDE in the first *XMM–Newton* observation. We also obtained a high-quality UV-optical spectrum with the Southern Astrophysical Research (SOAR) Telescope and put a very tight constraint on the persistent nuclear activity, with a persistent X-ray luminosity expected to be lower than the peak of the flare by a factor of >2700. Therefore, our multiwavelength follow-up observations strongly support the TDE explanation of the event.

Key words: accretion, accretion discs – black hole physics – galaxies: individual: 2XMMi J184725.1−631724 – X-rays: galaxies.

1 INTRODUCTION

Most supermassive black holes (SMBHs) at the centre of galaxies are quiescent, but they can sometimes reveal themselves by tidally disrupting and subsequently accreting stars that wander too close to them (Rees 1988, 1990; Komossa 2012, 2015). About 70 such tidal disruption events (TDEs) have been found thus far, with about 30 with X-ray detections (e.g. Komossa & Bade 1999; Gezari et al. 2012; Saxton et al. 2012; Maksym et al. 2013;

Miller et al. 2015).[1] While three hard TDEs discovered by *Swift* had peak X-ray luminosity L_X above 10^{48} erg s^{-1} and hard X-ray spectra (Bloom et al. 2011; Burrows et al. 2011; Cenko et al. 2012; Brown et al. 2015), most X-ray TDEs have peak $L_X \lesssim 10^{44}$ erg s^{-1} and pure thermal X-ray spectra of characteristic temperature $\lesssim 0.1$ keV. Some TDEs, such as 2XMMi J184725.1−631724 (hereafter J1847, Lin et al. 2011, hereafter Lin11) and XMMSL1 J074008.2−853927 (Saxton et al. 2017), seemed to have more complicated X-ray spectra, with an extra harder component besides the supersoft thermal component.

---

* E-mail: dacheng.lin@unh.edu

[1] https://tde.space/

Table 1. X-ray observations of J1847.

Observatory	Observation ID	Start date	Instrument	Exp[a] (ks)	$r_{\rm src}$[b] (arcsec)	Count Rate[c] (10^{-3} cts s^{-1})	$F_{\rm abs}$[d] (10^{-13} erg s^{-1} cm^{-2})	$F_{\rm unabs}$[d]	$L_{\rm bol}$[d] (10^{43} erg s^{-1})
XMM–Newton	0405550401(X1)	2006-09-06	pn	19.5	15	102 ± 2	2.2 ± 0.1	18 ± 3	1.81 ± 0.57
			MOS1	27.6	15	21.5 ± 0.9			
			MOS2	27.6	15	17.9 ± 0.8			
	0405380501(X2)	2007-04-16	pn	20.5	35	865 ± 6	19.2 ± 0.3	102 ± 9	6.40 ± 0.72
			MOS1	32.2	35	159 ± 2			
			MOS2	31.9	35	122 ± 2			
	0694610101(X3)[e,f]	2013-03-03	pn	19.1	20	<6.7	<0.25	<0.31	<0.98
			MOS1	25.6	20	<1.5			
			MOS2	25.5	20	<3.1			
Swift	00031930001(S1)	2011-02-23	XRT	5.0	20	<3.3	<1.5	<19	<6.1
	00031930002(S2)[e]	2013-04-05	XRT	3.1	20	<2.1	<1.2	<14	<7.6
	00031930003(S3)[e]	2013-04-07	XRT	2.8	20				
	00031930004(S4)[e]	2013-08-29	XRT	1.3	20	<3.4	<1.5	<18	<9.5
	00031930005(S5)[e]	2013-09-08	XRT	1.8	20				
	00031930006(S6)[e]	2015-03-15	XRT	1.4	20	<5.6	<2.1	<23	<18.8
Chandra	15637(C1)[e]	2013-03-29	ACIS-S	14.9	1.1	0.32 ± 0.15	$0.020^{+0.020}_{-0.012}$	$0.24^{+0.24}_{-0.15}$	$0.13^{+0.13}_{-0.08}$
ROSAT	800256(R1)	1992-10-11	PSPC	10.7	40	<2.3	<0.63	<0.87	<0.037

Notes. [a]*XMM–Newton* observations are all subject to background flares, the exposure times given are the clean exposure times after excluding periods of strong background flares.

[b]The radius of the source extraction region.

[c]The count rates correspond to different energy bands for different observatories (*XMM–Newton* in 0.2–10 keV, *Swift* in 0.3–10 keV, *Chandra* in 0.3–8 keV, and *ROSAT* in 0.1–2.4 keV), with 1σ errors or 3σ upper limits (calculated with the CIAO task `aprates`).

[d]The 0.2–10 keV absorbed ($F_{\rm abs}$) and unabsorbed ($F_{\rm unabs}$) fluxes and the unabsorbed bolometric luminosity $L_{\rm bol}$ (integrated over 0.001–100 keV) for X1 and X2 are taken from Lin11, based on the WABS*SIMPL(DISKBB) model. For the *ROSAT* observation R1, we assumed an absorbed PL of $\Gamma_{\rm PL} = 2.0$ and $N_{\rm H} = 8.5 \times 10^{20}$ cm^{-2} (the bolometric luminosity were integrated over 0.2–100 keV for this model). For all the other observations, we assumed the WABS*SIMPL(DISKBB) fit to X1, with the disc temperature adjusted based on the expected decrease in the bolometric luminosity (see the text for more details). Either 90 per cent errors or 3σ upper limits are given.

[e]New follow-up observations.

[f]For X3, the observed count rates, fluxes and the bolometric luminosity are treated as upper limits, given that in this observation J1847 was strongly contaminated by Source 2.

J1847 is among the four X-ray TDE candidates that we have discovered (Lin11; Lin et al. 2013, 2015, 2017a,b) in our project of classification of bright X-ray sources from the *XMM–Newton* catalogue (Lin, Webb & Barret 2012). It was serendipitously detected in two *XMM–Newton* observations (hereafter X1 and X2, Table 1) in the direction of the centre of the galaxy IC 4765-f01-1504 (Carrasco, Mendes de Oliveira & Infante 2006) at a redshift of 0.0353 ($D_L = 149$ Mpc, assuming a flat universe with $H_0 = 73$ km s^{-1} Mpc^{-1} and $\Omega_{\rm M} = 0.27$; Lin11). These two *XMM–Newton* observations were separated by 211 d, with the X-ray flux in X2 higher than in X1 by nearly one order of magnitude. The X-ray spectra in both observations are very soft and can be described by a model dominated by a cool (temperature $\lesssim 0.1$ keV) thermal disc component plus a weak steep (photon index $\Gamma_{\rm PL} \sim 3.5$) power law (PL), similar to the thermal state of stellar-mass black hole (BH) X-ray binaries (Remillard & McClintock 2006). The large amplitude (by a factor >64) of the flare is supported by the non-detection of the source in a *ROSAT* observation in 1992. The decay of the X-ray flare had been hinted by the non-detection of the source in a follow-up *Swift* observation ~ 4 yr after X2, which implied a flux decaying factor of $\gtrsim 12$. The host galaxy showed no clear sign of persistent nuclear activity, based on our Gemini spectrum taken in 2011, which showed no emission lines but typical stellar absorption features. The probable transient nature, extremely soft X-ray spectra, and an otherwise quiescent host prompted Lin11 to conclude that it is a TDE. The X-ray spectra of the TDE candidate XMMSL1 J074008.2−853927 are different from those of J1847 in that X-ray

spectra of XMMSL1 J074008.2−853927 are more similar to those typically seen in Seyfert galaxies, with the PL component being hard ($\Gamma_{\rm PL} \sim 2$) and strong (relative to the soft component, Saxton et al. 2017).

We have obtained more follow-up observations of J1847 from optical to X-rays, including one new *XMM–Newton* observation (hereafter X3, Tables 1 and 2), one *Chandra* observation (hereafter C1), five new *Swift* observations (hereafter S2–S6), and one Southern Astrophysical Research (SOAR) optical spectrum. Here we report the results of these new observations, which we find to further support the TDE nature of the event. In Section 2, we describe the observations and data analysis. In Section 3, we present the results. Our discussion on the source nature and conclusions are given in Section 4.

2 DATA ANALYSIS

2.1 The *XMM–Newton* and *Chandra* observations

The *XMM–Newton* observation X3 was taken on 2013 March 3 (Table 1) with a duration of 44 ks using the three European photon imaging cameras (i.e. pn, MOS1, and MOS2; Jansen et al. 2001; Strüder et al. 2001; Turner et al. 2001) in a full-frame mode. Strong background flares, which were seen in all cameras, were excluded

Table 2. The UV Photometry.

Observation ID	Start date	Filter	$\lambda_{\rm eff}$ (Å)	Exposure (ks)	Magnitude (AB mag)
XMM–Newton/OM:					
0405550401(X1)	2006-09-06	*UVW*1	2910	1.8	19.78 ± 0.09
		*UVM*2	2310	2.7	19.90 ± 0.11
0694610101(X3)[a]	2013-03-03	*UVW*1	2910	9.8	20.34 ± 0.06
		*UVM*2	2310	9.6	20.46 ± 0.08
		*UVW*2	2120	14.3	20.62 ± 0.13
Swift/UVOT:					
00031930001(S1)	2011-02-23	*UVW*1	2589	4.9	20.08 ± 0.05
00031930002(S2)[a]	2013-04-05	*UVW*1	2589	3.1	20.19 ± 0.07
00031930003(S3)[a]	2013-04-07	*UVW*2	2031	2.8	20.42 ± 0.06
00031930004(S4)[a]	2013-08-29	*UVW*2	2031	1.3	20.27 ± 0.08
00031930005(S5)[a]	2013-09-08	*UVW*2	2031	1.8	20.36 ± 0.07
00031930006(S6)[a]	2015-03-15	*UVW*2	2031	1.4	20.60 ± 0.09

Note. [a]New follow-up observations.

following the SAS thread for the filtering against high backgrounds.[2] After excluding the strong background intervals, we were left with only good exposures of 19.1, 25.6, and 25.5 ks for pn, MOS1, and MOS2, respectively (Table 1). There was some weak hard emission near the position of J1847. However, this hard source seems to be significantly offset from J1847. The offset is 4.8 arcsec and is larger than the 3σ positional uncertainty (3.4 arcsec) of the hard source, based on the 3XMM-DR6 catalogue (Rosen et al. 2016). In order to check whether this hard source is J1847, we requested the *Chandra* observation C1 (15 ks, Table 1) in the director's discretionary time program. The observation was made on 2013 March 29 (26 d after X3). It used the AXAF CCD Imaging Spectrometer (ACIS; Bautz et al. 1998), with the aimpoint and our target at the back-illuminated chip S3. We reprocessed the data to apply the latest calibration (CALDB 4.7.3) using the script `chandra_repro` in the CIAO version 4.9 (Chandra Interactive Analysis of Observations) package. No high background flares were seen in C1, and we used the data of the whole observation.

The *Chandra* image clearly resolved the emission near J1847 in X3 into two sources, one at the position of J1847, thus probably the same source, and the other only 5.9 arcsec away (hereafter Source 2). This offset was obtained based on our performance of the source detection on the 0.3–7 keV image binned at single sky pixel resolution with the CIAO `wavdetect` wavelet-based source detection algorithm (Freeman et al. 2002). We extracted the spectra and the corresponding response files for both sources using the CIAO task `specextract`. We used a circular source region enclosing 90 per cent of the point spread function (PSF) at 2.0 keV (radius 1.1 arcsec for both sources) and a circular background region of radius 20 arcsec near the sources.

Although J1847 cannot be resolved from Source 2 in X3, the observation can still provide enough statistics to constrain the properties of these sources, thanks to the long exposure and the large effective area of the observation. Therefore, we analysed the observation in the same way as for X1 and X2 (Lin11), except using SAS 16.0.0 and the calibration files of 2017 February. We extracted the source and background spectra for the blended emission of J1847 and Source 2 in X3. We used a source region of radius 20 arcsec (the same for all cameras) centred at the detection position in the 3XMM-DR6 catalogue. A large background region (radius

100 arcsec for MOS1 and MOS2 and radius 60 arcsec for pn) was used.

2.2 *Swift* observations

We also have six follow-up observations of J1847 with *Swift*, including the one in 2011 that had been analysed in Lin11 (Table 1). We analysed the six observations with FTOOLS 6.20 and the calibration files of 2017 February. In all observations, the X-ray telescope (XRT; Burrows et al. 2005) was operated in photon counting mode, and we reprocessed the data with the task XRTPIPELINE (version 0.13.3) to update the calibration. J1847 was not detected in the XRT in these observations. In order to obtain the constraint of the X-ray flux of the source in these observations, we extracted the source and background spectra using circular source and background regions of radii 20 and 100 arcsec, respectively. The 3σ upper limit on the count rate was estimated using the CIAO task `aprates`, which adopts the Bayesian approach. The UV-Optical Telescope (UVOT; Roming et al. 2005) in these observations used the ultraviolet (UV) filters *UVW*1 and *UVW*2 (Table 2), with a goal to monitor the UV emission. We used the task `uvotsource` with radii of 5 and 20 arcsec for the circular source and background regions, respectively, and the most recent UVOT calibration as described in Poole et al. (2008) and Breeveld et al. (2010, 2011) to obtain the UV photometry.

2.3 The SOAR spectroscopic observation

We obtained a new optical spectrum of the host galaxy of J1847 using the Goodman High-Throughput Spectrograph (Clemens, Crain & Anderson 2004) on the SOAR 4.1-m telescope on 2013 August 26. Seven separate 30 min exposures were obtained, interspersed with arc lamps and flats, for a total on-source exposure time of 3.5 h. For all data, we used the 400 l mm^{-1} grating, centred at about 5000 Å, for an approximate wavelength coverage of 3000–7000 Å. We used a 1.07-arcsec slit, giving a resolution of 6.8 Å. The individual exposures were reduced and optimally extracted, using apertures ranging from 2.07 to 2.31 arcsec, depending on the seeing in each exposure. Then the spectra from individual exposures were co-added to yield the final spectrum.

We used Penalized Pixel Fitting (PPXF) software (Cappellari & Emsellem 2004) to fit the spectrum with multicomponent models comprised of single-population synthetic spectra from Vazdekis

et al. (2010), spanning a grid of 48 ages between 0.06–14 Gyr and 7 metallicities [M/H] = {−2.32, −1.71, −1.31, −0.71, −0.40, 0.00, +0.22} . The PPXF software implements the penalized pixel-fitting method to extract the stellar kinematics or stellar population from spectra of galaxies, with a maximum penalized likelihood approach. A multiplicative polynomial of degree 10 was incorporated in the fit to account for possible calibration uncertainties. The spectrum was corrected for the Galactic dust reddening of $E(B − V)_G = 0.10$ mag (Schlegel, Finkbeiner & Davis 1998) before the fit.

2.4 Astrometry correction

We need to obtain the astrometrically corrected positions of J1847 in various X-ray images to check whether the source is consistent with the galactic origin. The X1 and X2 sources were astrometrically corrected by aligning the 3XMM–DR6 sources with the 2MASS astrometry using four and six X-ray–infrared (IR) matches, respectively (J1847 was not in these match lists used for astrometry correction). We used the astrometric correction method in Lin et al. (2016), by searching for the translation and rotation of the X-ray frame that minimize the total χ^2 of the matches (χ is the ratio of the X-ray–IR separation to the total positional error). The uncertainties of the translation and rotation and thus the systematic positional errors of the X-ray sources associated with the astrometry correction procedure were estimated using 200 simulations. The final source positional uncertainties include the statistical component, the systematic error associated with the astrometry correction procedure, and the systematic error of 0.37 arcsec (1σ) of the 3XMM-DR6 catalogue (Rosen et al. 2016), added in quadrature. We note that the contamination of Source 2 has negligible effects on the position of J1847 that we derived from X1 and X2. This is because Source 2 in these observations would have count rates lower than those of J1847 by factors of 14 and 130, respectively, if it had similar fluxes as observed in C1.

The positions of the sources in C1 were taken from the output of the source detection tool `wavdetect`. The positional uncertainties included the statistical component, calculated using equation (12) in Kim et al. (2007), and the absolution astrometric uncertainty of *Chandra* obtained in Rots & Budavári (2011). No large systematic astrometric offset was found for C1 when we applied the astrometric correction method of Lin et al. (2016) to compare it with the 2MASS sources.

In order to check the galactic origin of J1847, we used an archival Very Large Telescope (VLT) FORS1 *R*-band image, which resolves the candidate host galaxy of J1847 well. It was taken on 2006 April 16. We aligned the astrometry of the image with that of the 2MASS. The VLT image has a relatively small size of 6.8 × 6.8 arcmin², which is the reason why we did not use it to carry out astrometry correction for X-ray sources.

3 RESULTS

3.1 Deep X-ray follow-up

In the *Chandra* observation C1, we collected 5 counts and 17 counts for J1847 and Source 2, respectively, within 0.3–8 keV, with only 0.2 counts expected to be from the background in both cases. The 95 per cent positional uncertainties of both sources from this *Chandra* observation are marked in Fig. 1, which shows the VLT FORS1 *R*-band image (upper panel) and the *Chandra* image (lower panel) around the field of J1847. The *Chandra* position of J1847 is consistent with the galaxy centre within the 95 per cent uncertainty.
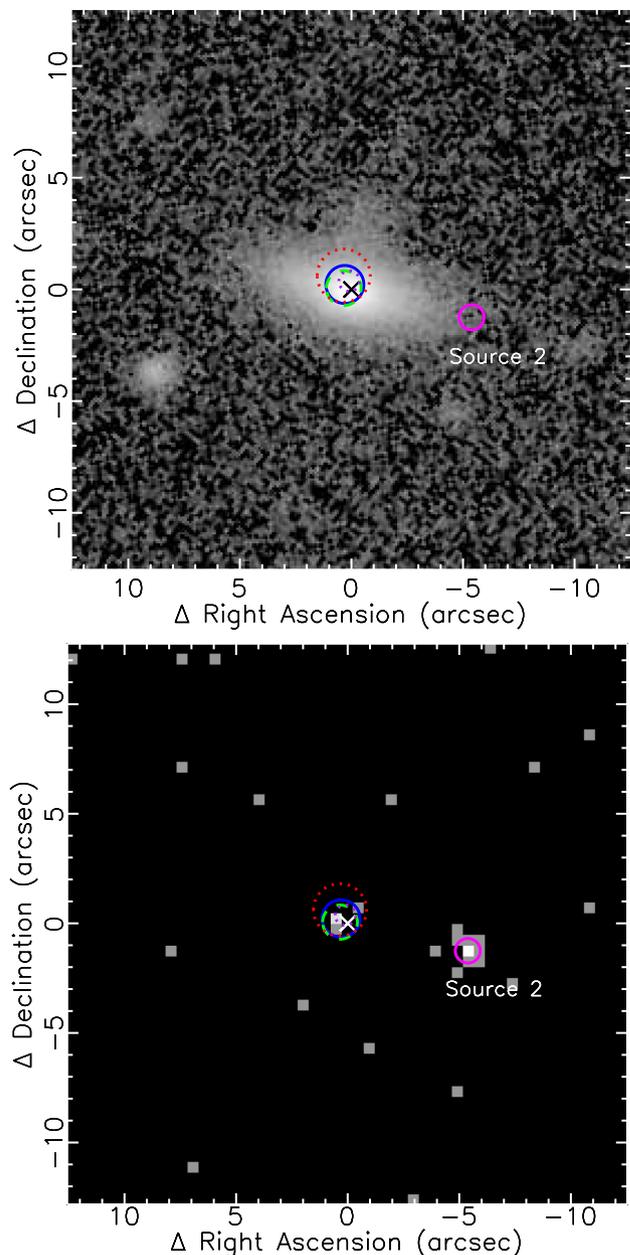
Figure 1. The VLT FORS1 *R*-band image (upper panel) and the *Chandra* X-ray image (C1, lower panel) around the field of J1847. The origins of the images are at the centre (black cross in the upper panel and white cross in the lower panel, R.A. = $18^h47^m25^s.12$, Dec. = $−63°17'25''.3$) of its host galaxy. The blue solid circle (radius 0.85 arcsec, i.e. 0.6 kpc, R.A. = $18^h47^m25^s.16$, Dec. = $−63°17'25''.1$) represents the 95 per cent positional uncertainty of J1847 from the *Chandra* observation C1. The green dashed circle (radius 0.78 arcsec, i.e. 0.5 kpc, R.A. = $18^h47^m25^s.17$, Dec. = $−63°17'25''.2$) is from the combination of *XMM–Newton* X-ray observations X1 and X2. The red dotted circle (radius 1.19 arcsec, i.e. 0.8 kpc, R.A. = $18^h47^m25^s.17$, Dec. = $−63°17'24''.7$) is from the UV observation in X1. The purple dotted circle (radius 0.46 arcsec, i.e. 0.3 kpc, R.A. = $18^h47^m25^s.13$, Dec. = $−63°17'24''.9$) is from the stacked *UVW*2 image of the *Swift* observations. The magenta solid circle (radius 0.56 arcsec, R.A. = $18^h47^m24^s.31$, Dec. = $−63°17'26''.6$) marks the 95 per cent positional uncertainty of Source 2, a nearby source detected in C1.
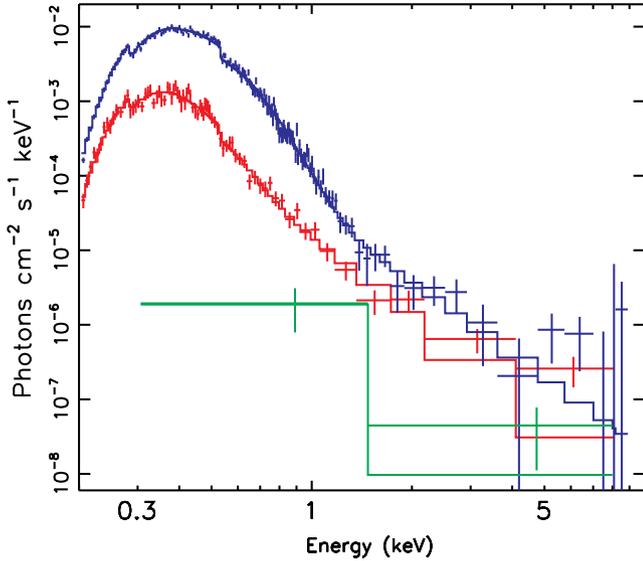
Figure 2. The X-ray spectra of J1847 from X2, X1, and C1 (from the top to the bottom). The X1 and X2 spectra were fitted with the WABS*SIMPL(DISKBB) model (from Lin11). For clarity, only pn spectra are shown. The model for C1 is the same as that of X2, except that the disc temperature was set to 35 eV (see the text).

It is also consistent with the average position (weighted by errors) from X1 and X2 (Fig. 1).

The very few counts of J1847 in the *Chandra* observation do not allow for a meaningful fit even with a simple model like an absorbed PL. The absorbed X-ray flux F_{abs} within 0.2–10 keV is fairly independent of the spectral shape. Assuming an absorbed PL of $N_H = 8.5 \times 10^{20}$ cm^{-2} (Lin11) and a large range of Γ_{PL} (2.0–5.0), we obtained $F_{abs} = (1.5–2.0) \times 10^{-15}$ erg s^{-1} cm^{-2}, a factor of ~1000 lower than the peak flux (in X2, Table 1). The corresponding unabsorbed 0.2–10 flux had a much larger range $[(2–20) \times 10^{-15}$ erg s^{-1} cm$^{-2}]$.

The bolometric luminosity L_{bol} is more relevant for the test of the TDE explanation for J1847, but it is very sensitive to the spectral model adopted. In Lin11, the X1 and X2 spectra were well fitted with the WABS*SIMPL(DISKBB) model, as plotted in Fig. 2. The absorption model WABS, the standard thermal disc model DISKBB and the empirical convolution Comptonization model SIMPL, in which a fraction of the input seed photons are converted into a PL (Steiner et al. 2009), can be found in the X-ray spectral fitting package XSPEC (Arnaud 1996). Based on this model, the main spectral change between X1 and X2 was the inner disc temperature kT_{disc}, as often observed in the thermal state of the accreting stellar-mass BH X-ray binaries (Remillard & McClintock 2006; Done, Gierliński & Kubota 2007). Therefore, we could construct a reasonable WABS*SIMPL(DISKBB) model for the C1 spectrum of J1847, as long as its L_{bol} and thus kT_{disc} can be inferred in some way. In the standard TDE theory, L_{bol} is expected to decay with the time t after the stellar disruption as $t^{-5/3}$ (Rees 1988; Phinney 1989). The solid line in Fig. 3 plots such a decay trend with the disruption time assumed to be one month before X1, which is reasonable, given that the rising time to the peak is expected to be ~1–2 months (Ulmer 1999; Guillochon & Ramirez-Ruiz 2015) for a small BH (~10^6 M$_\odot$, Lin11). Based on this model, we expect $L_{bol} = 1.5 \times 10^{42}$ erg s^{-1} at the time of C1. This luminosity can be matched if we adjust the WABS*SIMPL(DISKBB) fit to X1 to have $kT_{disc} = 35$ eV. The model constructed this way is fully consistent
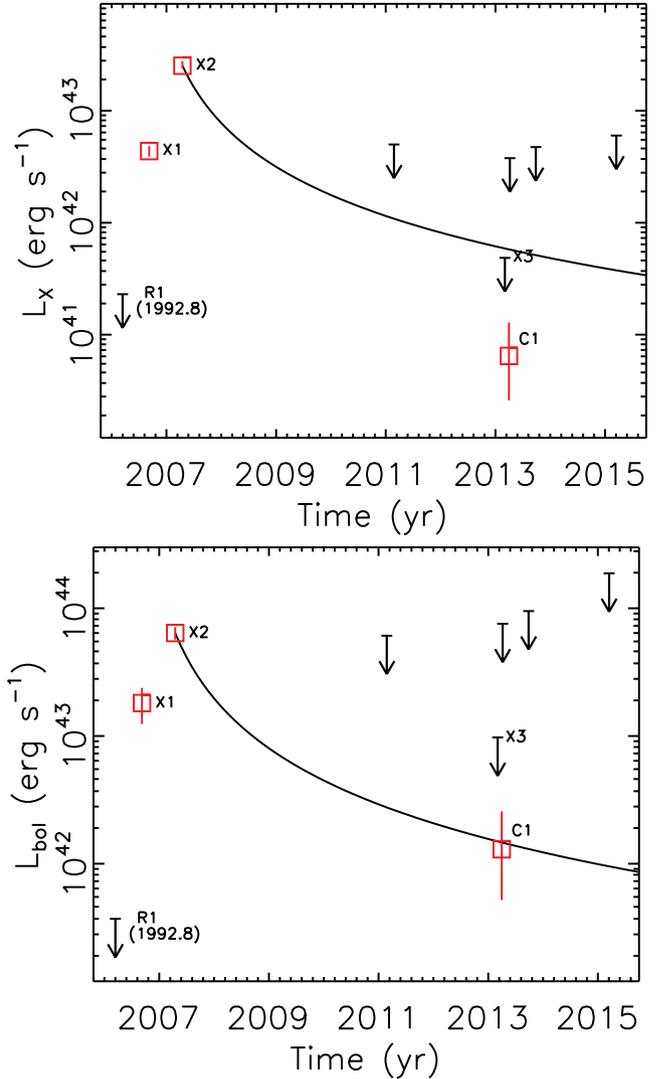

Figure 3. The long-term evolution of the unabsorbed X-ray (0.2–10 keV, upper panel) and bolometric (lower panel) luminosities of J1847. The squares with 90 per cent errors are detections, while the arrows represent 3σ upper limits (see Table 1 and Section 3.2 for more details). All observations are noted, except those from *Swift*. The solid line in both panel plots a typical TDE evolution curve $(t - t_D)^{-5/3}$, with t_D assumed to be one month before X1 and with X2 forced to be on the curve.

with the C1 spectrum, as shown in Fig. 2. The model predicts 3.3 counts, while we detected 4.8 net counts in C1.

Source 2 has enough counts for simple spectral fits. We binned the 0.3–8 keV spectrum to have at least 1 count per bin and fitted it with the *C* statistic (Cash 1979; Wachter, Leach & Kellogg 1979) in XSPEC with an absorbed PL model. We obtained $\Gamma_{PL} = 0.0^{+1.2}_{-0.7}$ (the error bars of the parameters from the spectral fits are at the 90 per cent confidence level throughout the paper), $N_H = 0.0^{+1.7} \times 10^{22}$ cm^{-2}, and a 0.3–8 keV absorbed flux of $f_{0.3–0.8 \, keV} = 2.8^{+1.7}_{-1.3} \times 10^{-14}$ erg cm^{-2} s^{-1}, indicating a faint X-ray source of a very hard spectrum.

In order to check whether there is large spectral and/or flux variability between X3 and C1, we also fitted the combined spectrum of J1847 and Source 2 from C1 with an absorbed PL and obtained $N_H = 0.0^{+0.8} \times 10^{22}$ cm^{-2}, $\Gamma_{PL} = 0.3 \pm 0.6$, and $f_{0.3–0.8 \, keV} = 3.2^{+2.0}_{-1.3} \times 10^{-14}$ erg cm^{-2} s^{-1}. These values are broadly consistent with those inferred in the fit to the combined 0.2–10 keV spectrum
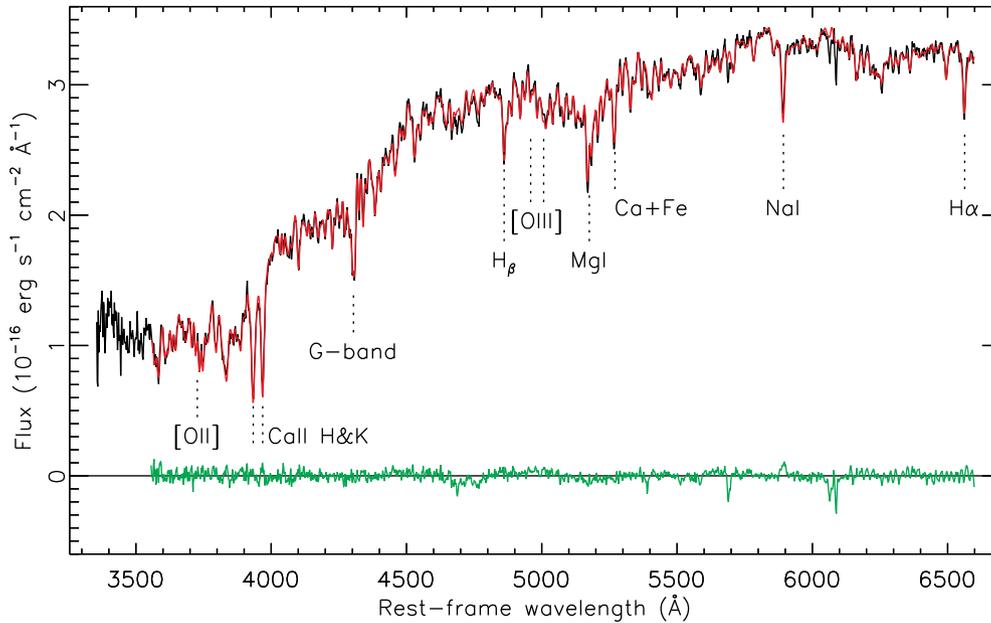
Figure 4. The SOAR optical/UV spectrum of the host galaxy of J1847 taken in 2013, showing no emission lines but typical stellar absorption features. The PPXF fit is shown as a red solid line, and the fit residuals are shown as a green solid line.

of J1847 and Source 2 from X3 ($N_H = 0.1^{+0.1} \times 10^{22}\,cm^{-2}$, $\Gamma_{PL} = 1.1 \pm 0.3$, and $f_{0.3-0.8\,keV} = 3.5 \pm 0.8 \times 10^{-14}\,erg\,cm^{-2}\,s^{-1}$). These parameters are broadly consistent with each other. Therefore, there should be no large flux and spectral change of both sources between X3 and C1. However, given the relatively large uncertainties of these parameters, we cannot rule out small variations like a factor of two in the total X-ray flux.

### 3.2 Long-term X-ray evolution

Fig. 3 shows the long-term evolution of the unabsorbed X-ray luminosity L_X (upper panel) of J1847 in 0.2–10 keV and the bolometric luminosity L_{bol} (lower panel). For X1 and X2, we used the luminosities inferred in Lin11 based on the WABS*SIMPL(DISKBB) model. Although the possible contamination of Source 2 on J1847 was not taken into account when we fitted the spectra of J1847 in X1 and X2, we found that the spectral fits obtained in Lin11 were hardly affected even if we included in the spectral fits an additional weak hard PL component with $\Gamma = 0.0$, as obtained in our fit to the spectrum of Source 2 in C1. The upper limit of the luminosity in the *ROSAT* observation was estimated assuming a typical spectrum of an active galactic nucleus (AGN), i.e. an absorbed PL of $N_H = 8.5 \times 10^{20}\,cm^{-2}$ (Lin11) and $\Gamma_{PL} = 2.0$ (Lin et al. 2012). For all the other observations, we assumed the WABS*SIMPL(DISKBB) fit to X1 with the disc temperature adjusted so that L_{bol} of the model matches that predicted in the standard TDE model (solid line in the lower panel in Fig. 3), as we did for C1 in Section 3.1. Except for X1, X2, and C1, in which the source was detected and had little contamination from Source 2, we calculated the 3σ upper limits for all other observations (Table 1). For X3, though J1847 was also detected in this observation, it was most likely seriously contaminated by Source 2. We therefore treated the total detected flux of Source 2 and J1847 as the upper limit of J1847 for this observation. We note that S2 and S3 are close in time and were thus combined to calculate the upper limit. This is also the case for S4 and S5.

The source clearly displayed a large variability in L_X, by a factor of $\sim$430 between X2 and C1, which were separated by $\sim$6 yr. The *Swift* observations are relatively shallow, and the non-detection of our source in these observations suggests that L_X might have decayed by a factor of $\gtrsim$5 from X2 since 2011. The variability of L_{bol} is somewhat less dramatic (a factor of 49 between X2 and C1) than that of L_X. This is due a larger bolometric correction for C1 than for X2. The C1 luminosity was estimated assuming a model of a much cooler disc ($kT_{disc} = 35$ eV, see Section 3.1) and thus a smaller fraction of photons in X-rays than the model used for X2 ($kT_{disc} = 93$ eV, Lin11).

3.3 Long-term optical and UV evolution

Fig. 4 shows the SOAR spectrum of the host galaxy of J1847. It exhibits no emission lines but typical stellar absorption features, as observed in the Gemini spectrum in 2011. The SOAR spectrum has much higher signal-to-noise ratio than the Gemini spectrum and can thus provide a much better constraint on the level of the nuclear activity. We obtained the 3σ upper limit of the luminosity of the [O III] λ5007 emission line to be $4.9 \times 10^{37}\,erg\,s^{-1}$. This limit has been corrected for Galactic reddening $E(B-V)_G = 0.10$ mag (Schlegel et al. 1998), but not the intrinsic reddening, which is probably very small given that the inferred column density from the X-ray spectral fit is close to the Galactic value (Lin11). Using the [O III] λ5007 and 2–10 keV luminosity relation in Lamastra et al. (2009), whose dispersion is 0.63 dex, we estimated the 3σ upper limit of the persistent unabsorbed 2–10 keV luminosity to be $4.2 \times 10^{39}\,erg\,s^{-1}$, or $1.0 \times 10^{40}\,erg\,s^{-1}$ in 0.2–10 keV, assuming a PL of $\Gamma_{PL} = 2.0$. This upper limit is a factor of $\sim$2700 lower than the peak luminosity (in X2).

Our PPXF fit of the spectrum over 3540–6600 Å (the source rest frame) is shown in Fig. 4. The fit inferred the intrinsic stellar velocity dispersion to be $118 \pm 14\,km\,s^{-1}$, which should be taken with caution because it is lower than the instrumental resolution of $\sim$170 km s^{-1}. The total stellar mass is $\sim$2.3 $\times 10^{10}$ M$_\odot$, and the
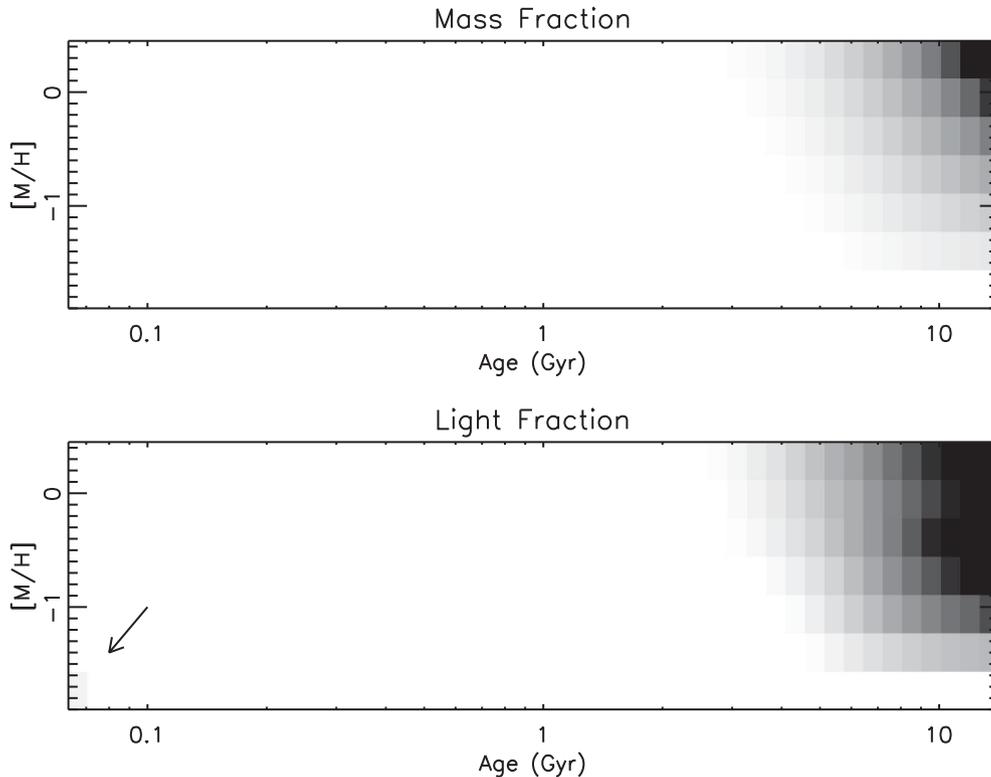
Figure 5. Relative mass and light fractions of different stellar populations in the host galaxy of J1847 with respect to metallicity and age. Darker shading indicates a larger mass/light fraction in the best-fitting model. The light was integrated over 3540–6600 Å. The plot shows that the host galaxy is dominated by very old (>10 Gyr) populations, but a very small young (<70 Myr) population (pointed with an arrow in the lower panel) seems to be present as well.

total luminosity within the fitting band is $\sim1.7 \times 10^9$ L$_\odot$, after correcting for the slit loss by matching the spectrum to the integrated V-band flux of the host galaxy obtained in Lin11. Therefore, the PPXF fit suggests a relatively low-mass galaxy.

The mass and light distributions of the stellar populations with respect to the age and the metallicity are shown in Fig. 5. The light-weighted age is 9.6 Gyr, and the mass-weighted is 10.3 Gyr, suggesting a galaxy dominated by old stellar populations.

The UV photometry of J1847 is given in Table 2. Our source fell in the field of view of the Optical Monitor (OM, Mason et al. 2001) in X1 and X3, but not in X2. Both X1 and X3 have been included in the third release of the XMM-OM Serendipitous Ultraviolet Source Survey Catalog (SUSS3, Page et al. 2012), which compiles all optical and UV sources detected in the OM between 2000 March and 2015 July, and the magnitudes of our source in Table 2 are from this catalogue. Both observations suggest the presence of a UV source at the position of J1847 (Fig. 1). This UV source appeared blue and variable. Both the *UVW*1 and *UVM*2 fluxes decreased from X1 to X3 by 0.6 mag at the 5σ and 4σ confidence levels, respectively. Because X1 was near the peak of the X-ray flare and had a much higher X-ray flux than X3, the UV enhancement in X1 is probably associated with the X-ray flare. The UV photometry from the *Swift* observations (Table 2) supports the presence of a blue UV source at the position of J1847, but it showed no clear variation in *Swift* observations. We note that the UV filter set in the UVOT is different from that of the *XMM–Newton* OM, so their photometry should not be directly compared with each other.

In the SUSS3 catalogue, the UV source was indicated as an extended source in *UVW*1 and *UVM*2 in X3 but not in X1. To check whether the UV source was extended in the *Swift* observations, we run the `uvotdetect` task in the FTOOLS in the stacked images, one

for each filter (*UVW*1 and *UVW*2). The task gave the profile root mean squares along the major and minor axes of the sources, from which we calculated a geometric mean r. From *UVW*1, we obtained $r = 1.07 \pm 0.03$ arcsec for point sources with similar magnitudes as J1847 and $r = 1.41$ arcsec for J1847, clearly suggesting that the UV source was extended (at the 10σ confidence level). For *UVW*2, we obtained $r = 1.13 \pm 0.03$ arcsec for point sources and $r = 1.23$ arcsec for J1847. Therefore, in this filter, there is some sign that the UV source was also extended, at the 3σ confidence level. In summary, both the X3 and *Swift* images suggest the extended nature of the UV source at the late time after the X-ray emission became very weak. We note that the UV source appeared symmetric and that there seemed to be no UV emission at the position of Source 2. Therefore, the extended nature of the UV source should not be caused by any contamination from Source 2.

4 DISCUSSION AND CONCLUSIONS

Our multiwavelength follow-up observations of J1847 support the TDE explanation of the source in several aspects. First, the X-ray monitorings of various observatories confirm the large amplitude of the X-ray outburst in 2006–2007, with the absorbed X-ray flux decaying by a factor of ~1000 six years after X2. Secondly, the optical spectrum of the host galaxy from the SOAR poses a very tight constraint on the persistent nuclear activity (persistent X-ray luminosity inferred to be $\lesssim 10^{40}$ erg s^{-1}), as supported by the X-ray observation C1. Thirdly, the C1 observation supports the nuclear origin of the event (<0.6 kpc).

Another support for the TDE explanation for J1847 is that the X-ray flux in C1 is fully consistent with that expected for a standard TDE, after properly taking into account the shifting of photon

energies out of the X-ray band due to the cooling of the disc (lower panel in Fig. 3, and Sections 3.1 and 3.2). The main result of this band-limited effect is that the X-ray luminosity has a steeper decay than the standard TDE trend of $t^{-5/3}$, as shown in the upper panel in Fig. 3. Lodato & Rossi (2011) showed that the X-ray spectral density at 0.2 keV could have an exponential decay, thus much steeper than the $t^{-5/3}$ decay, around a year after the stellar disruption. We note that our speculation for the presence of a strong cool disc in C1 and other follow-up observations does not conflict with our lack of the detection of the UV variability in *Swift* observations, because the UV emission from such a cool disc is expected to be an order of magnitude fainter than the extended UV emission detected, which could be due to a small young stellar population (see below).

There are other cases in which X-ray flux could have a steeper decay than $t^{-5/3}$. One is partial disruption of a centrally concentrated star. In this case, a large drop in the decay of the mass accretion rate could occur in the months after the flare peak (Guillochon & Ramirez-Ruiz 2013). Temporary large drops in the light curves of TDEs could also be caused by the presence of a secondary SMBH (Liu, Li & Chen 2009), as is probably the case for the TDE SDSS J120136.02+300305.5 (Liu, Li & Komossa 2014). We cannot completely rule out these explanations for the steeper decay of the X-ray flux than $t^{-5/3}$ in J1847 due to the poor sampling of the light curve.

We have mainly considered the faint emission of J1847 in C1 as due to the TDE, but we cannot rule it out as the pre-existing very faint AGN instead. The 0.2–10 keV luminosity of J1847 in C1 ($\sim$1.2 $\times$ 10^{40} erg s^{-1}, assuming an absorbed PL of $N_H = 8.5 \times 10^{20}$ cm^{-2} and $\Gamma_{PL} = 2.0$, typical of AGN spectra) is compatible with the 3σ upper limit (1.0 $\times$ 10^{40} erg s^{-1}) set by the SOAR optical spectrum. The emission in C1 is less likely to be due to the star-forming activity. The star formation rate of the host galaxy is about 0.2 M$_\odot$ yr^{-1} based on the *UVW*2 flux (corrected for the Galactic reddening, Hirashita, Buat & Inoue 2003). This rate implies a 0.5–10 keV luminosity of 10^{39} erg s^{-1} (Ranalli, Comastri & Setti 2003), significantly lower than observed in C1.

There is a blue UV source at the nucleus of the host galaxy of J1847. Given its probably extended nature in the observations after 2011 (X3 and S1–S6), this UV source could be due to the presence of a small young stellar population, as inferred in the PPXF fit to the SOAR spectrum (see the lower panel in Fig. 5). The probable decay of the UV source from X1 to X3 by $\sim$0.6 mag, however, requires significant contribution to the UV emission from the TDE in X1. The presence of a young stellar population at the nucleus is interesting, as it has been suspected that the TDE rate might be enhanced in young stellar environments (Arcavi et al. 2014; Tadhunter et al. 2017). Given the dominant very old stellar populations of the host, one possible explanation for the nuclear young stellar population might be a recent minor merger. The possible evidence of this minor merger could be the prominence to the north of J1847 in the VLT image (Fig. 1).

In Lin11, we ruled out J1847 as AGNs (based on the very soft X-ray spectra of J1847), foreground stars (based on the large X-ray-to-IR flux ratio of J1847, see also Lin et al. 2012) and Galactic supersoft X-ray sources (J1847 would be too faint to be such an object if it is in our Galaxy). The very large X-ray variability inferred from our follow-up observations and the extremely weak nuclear activity as indicated by the SOAR optical spectrum strengthen our arguments against the AGN explanation for J1847. J1847 is unlikely to be a γ-ray burst (GRB) or a supernova (SN), based on typical arguments applied to most X-ray TDEs of very soft X-ray spectra and high luminosities over a long time (e.g. Maksym, Lin & Ir-

win 2014; Lin et al. 2015, 2016). GRBs and SNe typically have very hard X-ray spectra, with $\Gamma_{PL} \lesssim 2$ (Immler 2007; Grupe et al. 2013; Levan et al. 2013). SNe could show luminous very soft X-ray spectra during the prompt shock breakouts (Soderberg et al. 2008), but this phase is expected to be short in time (less than hours, Nakar & Sari 2012), while J1847 at least stayed bright and supersoft for 0.6 yr. Some ultralong GRBs exhibited relatively soft late-time X-ray spectra ($\Gamma_{PL} \lesssim 5$), but they normally also had significant very hard X-ray emission above 2 keV (e.g. Piro et al. 2014; Margutti et al. 2015), but J1847 showed little emission above 2 keV and was much softer in X1 and X2, with $\Gamma_{PL} = 5.9$ and 6.9, respectively, when fitted with an absorbed PL.

Our *Chandra* observation C1 revealed a faint source (Source 2) only 6 arcsec away from J1847. This source appears to be in the galactic plane of the host galaxy of J1847, but no clear optical counterpart is seen in the VLT image (Fig. 1). If it is in this galaxy, it would have an absorbed 0.3–8 keV luminosity of 7×10^{40} erg s^{-1}, fulfilling the definition of an ultraluminous X-ray source ($>10^{39}$ erg s^{-1}, Feng & Soria 2011). However, it is very rare to have such a bright off-nuclear X-ray source in an early-type galaxy (Fabbiano 2006). One possible exception could be that there was a minor merger, with Source 2 corresponding to the tidal stripped nucleus of a merging dwarf galaxy (see Farrell et al. 2012; Lin et al. 2016). Although this explanation seems interesting, given that a minor merger could also explain the presence of a nuclear young stellar population (see above), it is still fairly speculative without high-resolution imaging of the environment. An alternative explanation for Source 2 is a background AGN. No matter whether it is an offset nucleus or a background AGN, it might have a Seyfert 2 type, given its very hard X-ray spectrum (Lin et al. 2012). We do not favour the explanation of Source 2 as a γ-ray burst or a SN, whose X-ray spectra typically have $\Gamma_{PL} \gtrsim 1.0$ (Grupe et al. 2013), not as hard as Source 2. We note that we cannot rule out Source 2 as a foreground Galactic source either. With a very hard X-ray spectrum, it could be an intermediate polar (Muno et al. 2004).

REFERENCES

Arcavi I. et al., 2014, ApJ, 793, 38
Arnaud K. A., 1996, in Jacoby G. H., Barnes J., eds, ASP Conf. Ser. Vol. 101, Astronomical Data Analysis Software and Systems V. Astron. Soc. Pac., San Francisco, p. 17

Bautz M. W. et al., 1998, in Hoover R. B., Walker A. B., eds, Proc. SPIE Conf. Ser. Vol. 3444, X-Ray Optics, Instruments, and Missions, SPIE, Bellingham, p. 210

Bloom J. S. et al., 2011, Science, 333, 203

Breeveld A. A. et al., 2010, MNRAS, 406, 1687

Breeveld A. A., Landsman W., Holland S. T., Roming P., Kuin N. P. M., Page M. J., 2011, in McEnery J. E., Racusin J. L., Gehrels N., eds, AIP Conf. Ser., Vol. 1358, Gamma Ray Bursts 2010, Am. Inst. Phys., New York, p. 373

Brown G. C., Levan A. J., Stanway E. R., Tanvir N. R., Cenko S. B., Berger E., Chornock R., Cucchiaria A., 2015, MNRAS, 452, 4297

Burrows D. N. et al., 2005, Space Sci. Rev., 120, 165

Burrows D. N. et al., 2011, Nature, 476, 421

Cappellari M., Emsellem E., 2004, PASP, 116, 138

Carrasco E. R., Mendes de Oliveira C., Infante L., 2006, AJ, 132, 1796

Cash W., 1979, ApJ, 228, 939

Cenko S. B. et al., 2012, ApJ, 753, 77

Clemens J. C., Crain J. A., Anderson R., 2004, in Moorwood A. F. M., Iye M., eds, Proc. SPIE, Vol. 5492, Ground-Based Instrumentation for Astronomy. SPIE, Bellingham, p. 331

Done C., Gierliński M., Kubota A., 2007, A&A Rev., 15, 1

Fabbiano G., 2006, ARA&A, 44, 323

Farrell S. A. et al., 2012, ApJ, 747, L13

Feng H., Soria R., 2011, New A Rev., 55, 166

Freeman P. E., Kashyap V., Rosner R., Lamb D. Q., 2002, ApJS, 138, 185

Gezari S. et al., 2012, Nature, 485, 217

Grupe D., Nousek J. A., Veres P., Zhang B.-B., Gehrels N., 2013, ApJS, 209, 20

Guillochon J., Ramirez-Ruiz E., 2013, ApJ, 767, 25

Guillochon J., Ramirez-Ruiz E., 2015, ApJ, 809, 166

Hirashita H., Buat V., Inoue A. K., 2003, A&A, 410, 83

Immler S., 2007, in Immler S., Weiler K., McCray R., eds, AIP Conf. Ser., Vol. 937, Supernova 1987A: 20 Years After: Supernovae and Gamma-Ray Bursters. Am. Inst. Phys., New York, p. 246

Jansen F. et al., 2001, A&A, 365, L1

Kim M. et al., 2007, ApJS, 169, 401

Komossa S., 2012, Eur. Phys. J. Web Conf., 39, 2001

Komossa S., 2015, J. High Energy Astrophys., 7, 148

Komossa S., Bade N., 1999, A&A, 343, 775

Lamastra A., Bianchi S., Matt G., Perola G. C., Barcons X., Carrera F. J., 2009, A&A, 504, 73

Levan A. J., Read A. M., Metzger B. D., Wheatley P. J., Tanvir N. R., 2013, ApJ, 771, 136

Lin D., Carrasco E. R., Grupe D., Webb N. A., Barret D., Farrell S. A., 2011, ApJ, 738, 52 (Lin11)

Lin D., Webb N. A., Barret D., 2012, ApJ, 756, 27

Lin D., Irwin J. A., Godet O., Webb N. A., Barret D., 2013, ApJ, 776, L10

Lin D. et al., 2015, ApJ, 811, 43

Lin D. et al., 2016, ApJ, 821, 25

Lin D., Godet O., Ho L. C., Barret D., Webb N. A., Irwin J. A., 2017a, MNRAS, 468, 783

Lin D. et al., 2017b, Nat. Astron., 1, 0033

Liu F. K., Li S., Chen X., 2009, ApJ, 706, L133

Liu F. K., Li S., Komossa S., 2014, ApJ, 786, 103

Lodato G., Rossi E. M., 2011, MNRAS, 410, 359

Maksym W. P., Ulmer M. P., Eracleous M. C., Guennou L., Ho L. C., 2013, MNRAS, 435, 1904

Maksym W. P., Lin D., Irwin J. A., 2014, ApJ, 792, L29

Margutti R. et al., 2015, ApJ, 805, 159

Mason K. O. et al., 2001, A&A, 365, L36

Miller J. M. et al., 2015, Nature, 526, 542

Muno M. P. et al., 2004, ApJ, 613, 1179

Nakar E., Sari R., 2012, ApJ, 747, 88

Page M. J. et al., 2012, MNRAS, 426, 903

Phinney E. S., 1989, in Morris M., ed., IAU Symp. 136, The Center of the Galaxy. Dwarfs. Kluwer, Dordrecht, p. 543

Piro L. et al., 2014, ApJ, 790, L15

Poole T. S. et al., 2008, MNRAS, 383, 627

Ranalli P., Comastri A., Setti G., 2003, A&A, 399, 39

Rees M. J., 1988, Nature, 333, 523

Rees M. J., 1990, Science, 247, 817

Remillard R. A., McClintock J. E., 2006, ARA&A, 44, 49

Roming P. W. A. et al., 2005, Space Sci. Rev., 120, 95

Rosen S. R. et al., 2016, A&A, 590, A1

Rots A. H., Budavári T., 2011, ApJS, 192, 8

Saxton R. D., Read A. M., Esquej P., Komossa S., Dougherty S., Rodriguez-Pascual P., Barrado D., 2012, A&A, 541, A106

Saxton R. D., Read A. M., Komossa S., Lira P., Alexander K. D., Wieringa M. H., 2017, A&A, 598, A29

Schlegel D. J., Finkbeiner D. P., Davis M., 1998, ApJ, 500, 525

Soderberg A. M. et al., 2008, Nature, 453, 469

Steiner J. F., Narayan R., McClintock J. E., Ebisawa K., 2009, PASP, 121, 1279

Strüder L. et al., 2001, A&A, 365, L18

Tadhunter C., Spence R., Rose M., Mullaney J., Crowther P., 2017, Nat. Astron., 1, 0061

Turner M. J. L. et al., 2001, A&A, 365, L27

Ulmer A., 1999, ApJ, 514, 180

Vazdekis A., Sánchez-Blázquez P., Falcón-Barroso J., Cenarro A. J., Beasley M. A., Cardiel N., Gorgas J., Peletier R. F., 2010, MNRAS, 404, 1639

Wachter K., Leach R., Kellogg E., 1979, ApJ, 230, 274

This paper has been typeset from a TEX/LATEX file prepared by the author.